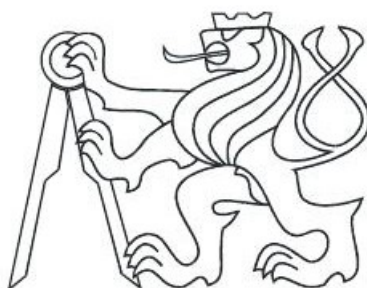


Czech Technical University in Prague
Faculty of Nuclear Sciences and Physical Engineering



**Study of Localised Particle Multiplicity Fluctuations
by Means of Wavelet and Multi-Resolution Analysis
in the Ultra-Relativistic Heavy Ion Collisions**

Bachelor's Thesis

Author: Jan Rusňák

Supervisor: doc. RNDr. Vojtěch Petráček, CSc.

Prague, 2008

název práce: **Studium lokalizovaných fluktuací multiplicity nabitých částic produkovaných v ultra-relativistických jaderných srážkách metodami vlnkové analýzy a analýzy s proměnným rozlišením**

autor: Jan Rusňák

obor: Jaderné inženýrství

druh práce: Bakalářská práce

vedoucí práce: doc. RNDr. Vojtěch Petráček, CSc. Katedra fyziky, Fakulta jaderná a fyzikálně inženýrská, České vysoké učení technické v Praze

konzultant: -

abstrakt: Při ultra-relativistických jaderných srážkách dochází k produkci velkého množství nabitých částic. Z prostorového rozložení jejich emise lze například detekovat výskyt předpokládaných jevů jako jsou disorientovaný chirální kondenzát, tzv. pionový laser nebo nalézt výtrysky částic (jety). Detekce malých oblastí se zvýšenou četností nabitých částic (domény) na pozadí několika tisíc dalších vzniklých částic vyžaduje aplikaci speciálních metod, mezi něž patří metody vlnkové (waveletové) analýzy a metody s proměnným rozlišením (MRA).

Cílem práce je seznámení (se) s možnostmi detektoru ALICE na urychlovači LHC a s problematikou aplikace waveletových a MRA metod při studiu produkce částic při jaderných srážkách v experimentu ALICE. Součástí práce jsou i simulace sloužící k ověření možností aplikace jedné z MRA metod.

klíčová slova: Chirální symetrie, chirální kondenzát, DCC, wavelet, vlnková analýza, analýza s proměnným rozlišením, MRA, ALICE

title: **Study of Localised Particle Multiplicity Fluctuations by Means of Wavelet and Multi-Resolution Analysis in the Ultra-Relativistic Heavy Ion Collisions**

author: Jan Rusňák

supervisor: doc. RNDr. Vojtěch Petráček, CSc.

consultant: -

abstract: Large amounts of charged particles are being produced during the ultra-relativistic nuclear collisions. Their spatial distribution can help us to detect particle jets, or some more exotic (hypothetical) phenomena, like disoriented chiral condensate (DCC) or pion laser. In order to detect small particle domains inside a large background, sophisticated analytical methods such as wavelet analysis or multi-resolution analysis (MRA) have to be used.

The main aim of this work is the familiarisation with the wavelet and multi-resolution analysis and application of one of the MRA method on simulated data in order to prove the MRA's abilities. Indispensable space will be also dedicated to the proprieties and potential of the detector ALICE at LHC.

key words: Chiral symmetry, chiral condensate, DCC, wavelet, multi-resolution analysis, MRA, ALICE

Prohlášení

Prohlašuji, že jsem svou bakalářskou práci vypracoval samostatně a použil jsem pouze podklady (literaturu, projekty, SW atd.) uvedené v příloženém seznamu. Nemám závažný důvod proti použití tohoto školního díla ve smyslu § 60 Zákona č.121/2000 Sb., o právu autorském, o právech souvisejících s právem autorským a o změně některých zákonů (autorský zákon).

V Praze dne 25.7.2008

Jan Rusňák

Contents

Preface	6
1 Physics Around the Disoriented Chiral Condensate	7
1.1 Chiral Symmetry	7
1.1.1 Introduction	7
1.1.2 Symmetries	7
1.1.3 Chiral Symmetry Breaking	10
1.1.4 Explicit Symmetry Breaking and Linear Sigma Model	12
1.1.5 Non-linear Sigma Model	15
1.2 Disoriented Chiral Condensate	16
1.2.1 Preliminary	16
1.2.2 Theoretical Models	16
1.2.3 DCC Signatures	19
1.2.4 Experimental Methods	21
1.2.5 Present Status	23
2 Multi-Resolution Analysis	24
2.1 Multi-Resolution Wavelet Analysis	24
2.1.1 Description	24
2.1.2 Wavelet Analysis in Particular Experiments	27
2.2 Multi-Resolution Lorentz Analysis	30
2.2.1 Description	30
2.2.2 Application of MRLA on Simulated Events	31
3 ALICE Experiment	39
3.1 Introduction	39
3.2 Detector Overview	40
3.2.1 ITS	40
3.2.2 TPC	40
3.2.3 TRD	40
3.2.4 TOF	41
3.2.5 HMPID	41
3.2.6 PHOS	41

3.2.7	FMS	41
3.2.8	PMD	41
3.2.9	FMD	41
3.2.10	ZDC	42
3.2.11	T0 and V0	42
3.3	ALICE and DCC	42
Summary and Conclusion		43
Bibliography		44

Preface

Chiral symmetry, an important symmetry of the strong interaction, exhibits an interesting behaviour. In the standard conditions it is spontaneously and explicitly broken. This means neither the Hamiltonian, nor its ground state posses the symmetry. But when the energy density is large enough (e.g. during an ultra-relativistic heavy ion collision), the symmetry could be restored. Many theoretical physicist believe there is a possibility that the system could (after it cools down) return to another state, than it is common for regular vacuum. A region of *pseudo* vacuum is formed. This state would be unstable and would come over to the vacuum-like state.

Such a transition would be followed by an emission of low momentum pions, which would be more probably charged, than neutral. These pion domains are being called *Disoriented Chiral Condensate*. Their detection could give us useful information about some proprieties of the QCD vacuum.

Unfortunately, DCC domains' detection is quite complicated. Special analytical methods have been developed during past years for this purpose. An example is the multi-resolution wavelet analysis (sometimes refered as the “wavelet analysis”), which has been used e.g. in the image processing before. Another method is represented by the multi-resolution Lorentz analysis (sometimes refered as the “multi-resolution analysis”). I will present here various simulations which will show us the abilities (and also disabilities) of this method.

There have been several DCC searching experiments since 1990's, but without any major success. However, this year LHC at CERN should become fully operational, giving us opportunities to study via the experiments ALICE, ATLAS, CMS and LHCb nuclear collisions at enormous energies, far beyond the capacities of all contemporary colliders. Especially the detector ALICE could give us the answer, if the DCC exists or not.

Chapter 1

Physics Around the Disoriented Chiral Condensate

1.1 Chiral Symmetry

1.1.1 Introduction

Chiral symmetry is an important symmetry of the QCD Lagrangian in the limit of vanishing quark masses and is associated with the strong interaction. However, as we know, quarks are not massless. Thus it's only an approximate symmetry. But its application still yields meaningful results, because masses of the two lightest quarks (u,d) are small in comparison with hadronic scales. Interesting feature of the chiral symmetry is its spontaneous breakdown. This means that while the Hamiltonian possesses the symmetry, its ground state does not. An important consequence of the spontaneous breakdown of a symmetry is the existence of a massless mode, the so called Goldstone boson. In our case, the Goldstone boson is identified with the pion.

Under specific conditions (very high temperature), the chiral symmetry can be restored. This means that both the Hamiltonian and it's (high temperature) state possess the symmetry. After the symmetry restoration, there are no Goldstone modes present. Thus the pions will become as heavy as hadrons (if the matter is still confined). Later, while the system is cooling down, the symmetry spontaneously breaks once again. These are the conditions, when the disoriented chiral condensate can be formed up.

1.1.2 Symmetries

A very nice concept of the chiral symmetry is described in [5]. This section is a short summary of the cited article.

Lagrangian formulation has one advantage. Symmetries of the Lagrangian lead to conserved quantities - currents. For example, we know from classical mechanics that space

invariance of the Lagrange function leads to conserved momentum, time invariance implies energy conservation.

Imagine a transformation of the fields

$$\Phi \rightarrow \Phi + \delta\Phi \quad (1.1)$$

Let the Lagrange function is invariant under the transformation (1.1)

$$\mathcal{L}(\Phi) = \mathcal{L}(\Phi + \delta\Phi) \quad (1.2)$$

This can be rewritten as

$$0 = \mathcal{L}(\Phi + \delta\Phi) - \mathcal{L}(\Phi) \quad (1.3)$$

We can expand the (1.3) to the first order in $\delta\Phi$

$$0 = \frac{\partial\mathcal{L}}{\partial\Phi}\delta\Phi + \frac{\partial\mathcal{L}}{\partial(\partial_\mu\Phi)}\delta(\partial_\mu\Phi) \quad (1.4)$$

Using this equation together with Hamilton's principle of the lowest action and Lagrange's equations of motion yields

$$0 = \partial_\mu \left(\frac{\partial\mathcal{L}}{\partial(\partial_\mu\Phi_i)}\delta\Phi_i \right) \quad (1.5)$$

This means that the quantity

$$J_\mu = \frac{\partial\mathcal{L}}{\partial(\partial_\mu\Phi_i)}\delta\Phi_i \quad (1.6)$$

is a conserved current ($\partial^\mu J_\mu = 0$) for possible fields Φ_i .

Let's take a look what happens with the Lagrangian of two-flavours massless fermions. It is given by

$$\mathcal{L} = i\bar{\psi}_i\partial_\mu\gamma^\mu\psi_i \quad (1.7)$$

Now consider the transformation

$$\Lambda_V : \psi \rightarrow e^{-i\frac{\vec{\tau}}{2}\vec{\Theta}}\psi \simeq \left(1 - i\frac{\vec{\tau}}{2}\vec{\Theta}\right)\psi \quad (1.8)$$

where ψ is now a spinor $\begin{pmatrix} u \\ d \end{pmatrix}$ and $\vec{\tau}$ are usual Pauli isospin matrices. Transformation Λ_V of the $\bar{\psi}$ is

$$\bar{\psi} \rightarrow e^{i\frac{\vec{\tau}}{2}\vec{\Theta}}\bar{\psi} \simeq \left(1 + i\frac{\vec{\tau}}{2}\vec{\Theta}\right)\bar{\psi} \quad (1.9)$$

It holds

$$i\bar{\psi}\partial_\mu\gamma^\mu\psi \rightarrow i\bar{\psi}\partial_\mu\gamma^\mu\psi - i\vec{\Theta} \left(\bar{\psi}i\partial_\mu\gamma^\mu\frac{\vec{\tau}}{2}\psi - \bar{\psi}\frac{\vec{\tau}}{2}i\partial_\mu\gamma^\mu\psi \right) = i\bar{\psi}\partial_\mu\gamma^\mu\psi \quad (1.10)$$

consequently the Lagrangian \mathcal{L} is invariant under the transformation Λ_V and the associated conserved current (“vector current”) is equal to

$$V_\mu^a = \bar{\psi}\gamma_\mu\frac{\tau^a}{2}\psi \quad (1.11)$$

Let me realise another transformation, Λ_A

$$\Lambda_A : \psi \rightarrow e^{-i\gamma_5\frac{\vec{\tau}}{2}\vec{\Theta}}\psi \simeq \left(1 - i\gamma_5\frac{\vec{\tau}}{2}\vec{\Theta}\right)\psi \quad (1.12)$$

and

$$\bar{\psi} \rightarrow e^{-i\gamma_5\frac{\vec{\tau}}{2}\vec{\Theta}}\bar{\psi} \simeq \left(1 - i\gamma_5\frac{\vec{\tau}}{2}\vec{\Theta}\right)\bar{\psi} \quad (1.13)$$

The transformation of Lagrangian reads

$$\begin{aligned} i\bar{\psi}\partial_\mu\gamma^\mu\psi &\rightarrow i\bar{\psi}\partial_\mu\gamma^\mu\psi - i\vec{\Theta}\left(\bar{\psi}i\partial_\mu\gamma^\mu\gamma_5\frac{\vec{\tau}}{2}\psi + \bar{\psi}\gamma_5\frac{\vec{\tau}}{2}i\partial_\mu\gamma^\mu\psi\right) \\ &= i\bar{\psi}\partial_\mu\gamma^\mu\psi \end{aligned} \quad (1.14)$$

where we used anti-commutation relation $\gamma_\mu\gamma_5 = -\gamma_5\gamma_\mu$. In other words, the Lagrangian is invariant under the transformation Λ_A too. The conserved current is now called “axial-vector current”

$$A_\mu^a = \bar{\psi}\gamma_\mu\gamma_5\frac{\tau^a}{2}\psi \quad (1.15)$$

As we can see, the Lagrangian of massless fermions, or more generally, the massless QCD is invariant under the transformations Λ_V and Λ_A . This Lagrangian’s invariations are what is called the “Chiral symmetry”¹. But the situation will change if we introduce a mass term

$$\delta\mathcal{L} = -m(\bar{\psi}\psi) \quad (1.16)$$

The Lagrangian is now still invariant under the transformation Λ_V , but for Λ_A we get

$$\Lambda_A : m(\bar{\psi}\psi) \rightarrow m(\bar{\psi}\psi) - 2im\vec{\Theta}\left(\bar{\psi}\frac{\vec{\tau}}{2}\gamma_5\psi\right) \quad (1.17)$$

Then \mathcal{L} is not invariant under the axial transformation. Therefore Λ_A is not the exact symmetry, if the fermions (quarks) have a finite mass. However, at least masses of the u and d quarks are (compared to the constant $\Lambda_{QCD} \simeq 200MeV$) very small. Thus the symmetry can be understood as an approximate symmetry. One would also expect that in this case the axial current will be only partially conserved.

¹As “chiral symmetry” is often branded only the axial-vector symmetry, because what makes the chiral symmetry important are just the special properties of the axial-vector symmetry. I will try to distinguish these terms in the text properly.

1.1.3 Chiral Symmetry Breaking

Motivation

First, let me define the pionic field and the sigma field, which are representing the pions and the sigma particle.

$$\begin{aligned}\vec{\pi} &\equiv i\bar{\psi}\vec{\tau}\gamma_5\psi \\ \sigma &\equiv \bar{\psi}\psi\end{aligned}\tag{1.18}$$

Under Λ_V the pionic field transforms as

$$\vec{\pi} \rightarrow \vec{\pi} + \vec{\Theta} \times \vec{\pi}\tag{1.19}$$

Other words, it is rotated in the isospin space by the angle Θ . Thus the vector transformation is nothing else but the isospin rotation. The conserved current can be identified with the isospin current, which is (as we know from experiments) in the strong interaction really conserved.

On the other hand for Λ_A it can be shown that it reads

$$\Lambda_A : \vec{\pi} \rightarrow \vec{\pi} + \vec{\Theta}\sigma\tag{1.20}$$

and analogically

$$\sigma \rightarrow \sigma - \vec{\Theta}\vec{\pi}\tag{1.21}$$

This means under the axial-vector transformation the pi and sigma mesons are rotated into each other.

We have seen that Λ_A is a symmetry of the QCD Lagrangian (and Hamiltonian). Thus one could expect that mesons which can be rotated into each other by this transformation should have the same masses. However this is actually not our case. Mass of the π meson is approximately 140MeV. Mass of the sigma meson is expected to be about 400-1200MeV²). Such a big mass difference cannot be explained by the small symmetry breaking caused by the non-vanishing quark masses. Does it mean the axial symmetry is a nonsense? No, there are pieces of evidence (weak pion decay, so-called Goldberger-Treiman relation [5][6], and others) that the axial symmetry is a symmetry of the strong interaction and must be present somehow. So is there any solution? Yes, it is: the **spontaneous breakdown of the symmetry**.

²According to the Particle Data Group. Till now, sigma meson wasn't discovered. If it exists, it will probably be a wide resonance with full width $\Gamma = 600-1000\text{MeV}$.

Spontaneous Symmetry Breaking

A symmetry is spontaneously broken, if it doesn't realise itself in the Hamiltonian's ground state. This situation can be clearly demonstrated on an example from the classical mechanics. Imagine a parabolic cone (or a hemisphere) with a small ball tumbling inside. Such a potential has its minimum (and its ground state) just in the middle. This potential is obviously symmetric towards rotations around the z axis. That is how an unbroken symmetry looks like. Now consider another situation: a potential shaped like a Mexican hat with a ball placed on the top of it. The symmetry is unbroken, but the system is not in the ground state. As soon as possible the ball will (due to the gravitation force, in this "classical mechanics example") roll down (to the ground state) to whatever side. The ball is in the middle no more and the rotational symmetry has been spontaneously broken. However, the symmetry has still an influence on the system. Rotations around the z -axis (moving the ball inside the valley) cost us no energy. These motions can be identified as rotational excitations and - as we have said - they are not energy-consuming. On the other hand, the radial excitations (moving the ball up to the hill) do us cost some energy. Following pictures should be illustrative enough.

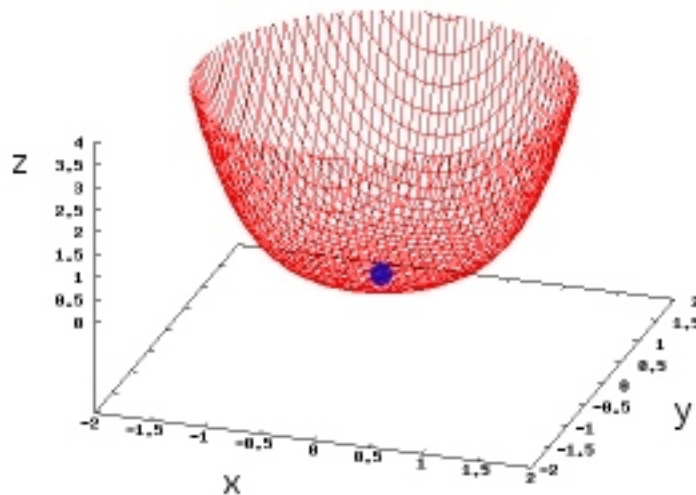


Figure 1.1: Rotationally invariant potential with unbroken symmetry

Let's return to the axial-vector symmetry now. We have shown that one expects the axial-vector symmetry to be spontaneously broken. So how would look an analogical picture to [Figure 1.2](#) like? It's quite straightforward. We just replace the axis x and y by the fields σ and $\vec{\pi}$ ³⁾. In this picture, the Λ_A transformation corresponds to the rolling of

³Actually, there should be 3 axes representing $\vec{\pi}$ (instead of one), but a 5-D graph is not easy to illustrate...

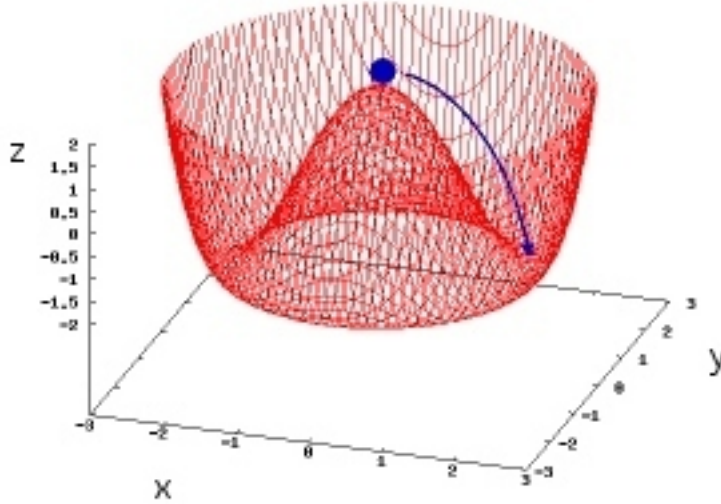


Figure 1.2: Spontaneous symmetry breaking

the ball inside the valley. For example, moving the ball from point $[2,0]$ to point $[0,2]$ could represent a transformation from the σ -state to one of the $\vec{\pi}$ -states.

The ground state now lies in the “valley”, not in the centre $([0,0])$. Hence one of the fields σ and $\vec{\pi}$ must have nonzero expectation value. It has to be the σ -field since it carries the quantum numbers of the vacuum. Consequently, the scalar quark condensate $\langle \bar{q}q \rangle$ will have a finite, non-vanishing value.

In this scheme, pionic states are only rotational excitations of the sigma state. As we have said, these excitations cost no energy. Therefore the pions should be massless. On the other hand, since excitations in the sigma direction are radial excitations, they are massive.

A general theorem - called the Goldstone Theorem - exists showing that whenever a continuous symmetry is broken spontaneously, massless particles appear in the spectrum of the theory. The resultant massless particles are called *Goldstone particles*. Thus pions are the Goldstone bosons of spontaneously broken chiral symmetry. In the real world, however, pions have some finite mass and are denoted as the *pseudo-Goldstone bosons*. How can be achieved these proprieties? It can be acquired by adding an **explicit symmetry breaking** term. Don't get confused - explicit breaking is a different effect than spontaneous breaking! What it is and what it brings will be discussed in the following section.

1.1.4 Explicit Symmetry Breaking and Linear Sigma Model

The linear sigma model (LSM) has its roots in the early 1960's. The Lagrangian which we will start with has to be Lorentz-scalar and invariant under the both Λ_A and Λ_V

transformations. In equations (1.19), (1.20) and (1.21) we have convinced ourselves that the $\vec{\pi}$ -field is invariant neither under Λ_V nor Λ_A transformation. Also the sigma field isn't invariant under the axial-vector transformation. However, for the squares of the fields one gets

$$\begin{aligned}\Lambda_V : \vec{\pi}^2 &\rightarrow \vec{\pi}^2 \\ \sigma^2 &\rightarrow \sigma^2\end{aligned}\tag{1.22}$$

and

$$\begin{aligned}\Lambda_A : \vec{\pi}^2 &\rightarrow \vec{\pi}^2 + 2\sigma\Theta_i\pi_i \\ \sigma^2 &\rightarrow \sigma^2 - 2\sigma\Theta_i\pi_i\end{aligned}\tag{1.23}$$

If we sum these squares, we will obtain

$$\Lambda_A, \Lambda_V : (\vec{\pi}^2 + \sigma^2) \rightarrow (\vec{\pi}^2 + \sigma^2)\tag{1.24}$$

It means we have found a term which is invariant under the transformation Λ_V and Λ_A as well. What more, it is a Lorentz-scalar. So we have found a good base for our Lagrangian. After a few steps (for more detailed description see e.g. [5]) one gets the final form of the Lagrangian

$$\begin{aligned}\mathcal{L} = & i\bar{\psi}\partial_\mu\gamma^\mu\psi - g_\pi (i\bar{\psi}\gamma_5\vec{\tau}\psi\vec{\pi} + \bar{\psi}\psi\sigma) \\ & - \frac{\lambda}{4} (\pi^2 + \sigma^2 - f_\pi^2)^2 + \frac{1}{2}\partial_\mu\pi\partial^\mu\pi + \frac{1}{2}\partial_\mu\sigma\partial^\mu\sigma\end{aligned}\tag{1.25}$$

with pion-nucleon coupling constant g_π and sigma-field's finite vacuum expectation value f_π :

$$f_\pi = \langle\sigma\rangle\tag{1.26}$$

The third term, namely

$$V = \frac{\lambda}{4} (\pi^2 + \sigma^2 - f_\pi^2)^2\tag{1.27}$$

is a pion sigma potential (“Mexican hat”) which is responsible for the finiteness of the $\langle\sigma\rangle$. As we can see, there are no explicit mass terms for the pi- and sigma-field in (1.25). But they could arise from an interaction with $\langle\sigma\rangle$. What are we going to do now is to introduce small fluctuations of the sigma- and pi-field around the ground state⁴) and to expand the potential (1.27) in them.

$$\sigma = f_\pi + (\delta\sigma) \text{ and } \pi = 0 + (\delta\pi)\tag{1.28}$$

$$V = \frac{\lambda}{4} ((\delta\pi)^2 + (f_\pi + \delta\sigma)^2 - f_\pi^2)^2 \simeq \lambda f_\pi^2 (\delta\sigma)^2\tag{1.29}$$

⁴These fluctuations are what we see to be the physical sigma (if sigma meson would be ever observed) and pi mesons

Terms of the third and higher orders have been neglected in the last step. One can then identify the mass of the sigma meson to be

$$m_\sigma^2 = 2\lambda f_\pi^2 \quad (1.30)$$

Since $\langle \pi \rangle = 0$ the mass of the pion must be zero. Which is in an agreement with our previous conclusion that the pions are Goldstone bosons of the spontaneous broken chiral symmetry. So how to get a non-vanishing mass for the pions? There must act some additional breaking of the symmetry - the explicit breaking.

Explicit Symmetry Breaking

There is a one big difference between the spontaneous and explicit symmetry breaking. While in the case of spontaneous symmetry breakdown the Hamiltonian's ground state is not symmetric, but the Hamiltonian itself still symmetric is, in the case of the explicit breakdown also the Hamiltonian is unsymmetric.

Such an explicit symmetry breaking is in the QCD carried out by the quark mass term

$$\delta\mathcal{L}_{QCD} = -m\bar{q}q \quad (1.31)$$

If we identify the quark condensate with the sigma-field (as we have done yet earlier), we can anticipate the breaking term of the LSM to have the following form

$$\delta\mathcal{L}_{LSM} = \varepsilon\sigma \quad (1.32)$$

with a symmetry breaking parameter ε . Since quark masses (at least u and d) are tiny, we expect only a small explicit symmetry breaking and hence only small value of the ε . The potential (1.27) now reads

$$V = \frac{\lambda}{4} (\pi^2 + \sigma^2 - V_0^2)^2 - \varepsilon\sigma \quad (1.33)$$

with a new parameter V_0 which satisfies $V_0 = f_\pi$ for $\varepsilon \rightarrow 0$. If the minimum shall still be at f_π , then V_0 has to be

$$V_0 = f_\pi - \frac{\varepsilon}{2\lambda f_\pi^2} \quad (1.34)$$

Same as before, only the axial-vector symmetry is broken. The vector symmetry stays unaffected. To get a better notion of what are we speaking about, an explicitly broken potential is displayed on [Figure 1.3](#). As a result of the introduction of the breaking term, the mass of the sigma meson has changed a bit

$$m_\sigma^2 = \frac{\partial^2 V}{\partial \sigma^2} |_{f_\pi} = 2\lambda f_\pi^2 + \frac{\varepsilon}{f_\pi} \quad (1.35)$$

and so have done the m_π

$$m_\pi^2 = \frac{\partial^2 V}{\partial \pi^2} |_{f_\pi} = \frac{\varepsilon}{f_\pi} \neq 0 \quad (1.36)$$

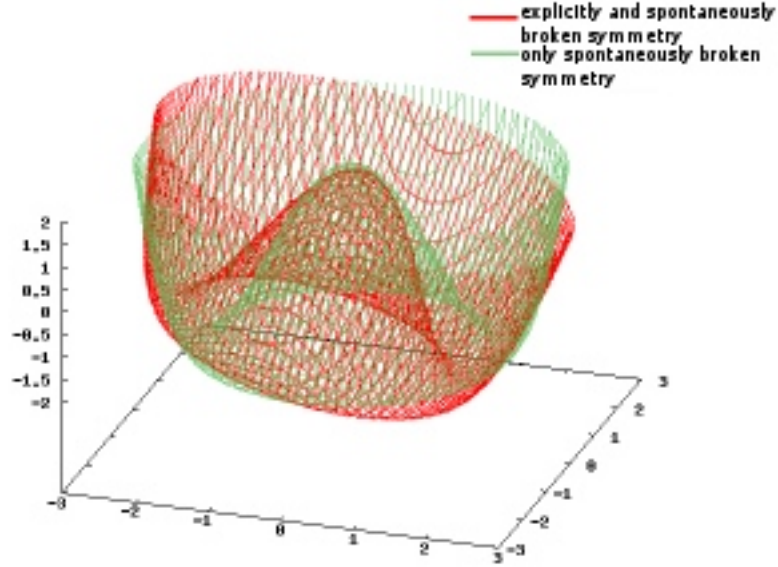


Figure 1.3: Example of an explicit symmetry breaking

Thus for the value of ε we get

$$\varepsilon = f_\pi m_\pi^2 \quad (1.37)$$

and the mass of the sigma meson becomes

$$m_\sigma^2 = 2\lambda f_\pi^2 + m_\pi^2 \quad (1.38)$$

The pion has now a non-vanishing mass, proportional to the square root of the explicit symmetry breaking parameter. This was our aim.

At this place I would like to make a final conclusion of the foregoing lines. Small, but non-vanishing quark masses are source of the explicit axial-vector symmetry breaking. Effects of this breaking, however, are small compared to the ones sequent upon the spontaneous symmetry breaking. Therefore our previous results derived for a system with spontaneously broken symmetry are still approximately valid and the system's dynamics will arise from the spontaneous symmetry breaking. Mass of the sigma meson is lifted a bit, but what is more important, the π -meson has now a nonzero mass, in agreement with the experiment.

1.1.5 Non-linear Sigma Model

At the end of this sub-chapter I would like to outline some basic ideas about the non-linear sigma model. Results of the linear sigma model are at the first sight just what we need, so why to set up other theories? The problem is that the LSM counts with the existence of an inconsistent particle - the sigma meson. And, as we said earlier, the σ -meson hasn't been

experimentally observed. The non-linear sigma model (NSM) doesn't demand existence of such a particle. This feature is achieved by sending the sigma meson's mass to the infinity. This can be done by considering infinite coupling constant λ in the potential (1.33). The "Mexican hat" will in consequence become steeper, with infinitely high walls. In such a potential, only pionic excitations (around the bottom) are allowed, radial excitations in the sigma direction are prohibited. The dynamics is now restricted to the bottom of the "hat" (so called chiral circle) only.

Subsequently the sigma-field disappears from the Lagrangian and the coupling between pions and nucleons is changed to a iso-vector coupling.

1.2 Disoriented Chiral Condensate

1.2.1 Preliminary

Ultra-relativistic heavy-ion collisions provide sufficient conditions (temperatures over a "chiral transition temperature") for chiral symmetry restoration. This means the pion sigma potential will be shaped as the one showed on Figure 1.1. After some period of time, when the system cools down, the symmetry is spontaneously broken once again. Since the beginning of the 1990's there have been opinions among the physicists that in such environment a region of pseudo-vacuum with its chiral order parameter tilted from the vacuum direction could appear. When these regions get in contact with the regular vacuum they dispose of their superfluous energy by coherent emission of low-energy pions. These regions are what is called the disoriented chiral condensate (DCC). One anticipates DCC presence will result in large event-by-event fluctuations of the charged-to-neutral rate of produced pions. Unfortunately, the DCC domains are expected to be very small, thus the neutral pion fraction fluctuations will occur only in small phase-space areas. This makes any eventual detection very difficult.

1.2.2 Theoretical Models

Baked Alaska

In order to get some intuitive understanding of the DCC, we will start this section with the Bjorken's original "Baked Alaska" model⁵). Let's have a high-energy heavy ion collision with high transverse energy deployed in the reaction zone, but with no high- p_T jets being formed. Thus the hadronization time can be quite long (a few fm/c). Most of the energy is carried out by the primary partons expanding to all directions at nearly speed of light. This means there is a hot, thin shell surrounding "cold" core. If energy density left inside the fireball decreases to values of order of tens of MeV/fm^3 , one can expect that the core

⁵"Baked Alaska" is a dessert made of ice cream placed in a pie dish lined with slices of sponge cake or pudding. The entire dessert is then placed in an extremely hot oven for just long enough to firm the meringue. The meringue is an effective insulator, and the short cooking time prevents the heat from getting through to the ice cream.

area will be similar to ordinary vacuum. However, if everything happens fast enough, the quark condensate can be rotated from its normal direction, since the energy density is still sufficient for compensating the effects of the explicit chiral symmetry breaking. After the outer shell hadronizes, the interior gets into contact with the surrounding vacuum and the disoriented quark condensate returns to the sigma-direction (from $(\vec{\pi}, \sigma)$ to $(\vec{0}, \sigma)$) in the chiral space, since it's the direction of the vacuum quark condensate. As a result, low-energetic pions are being emitted, with strong isospin correlations.

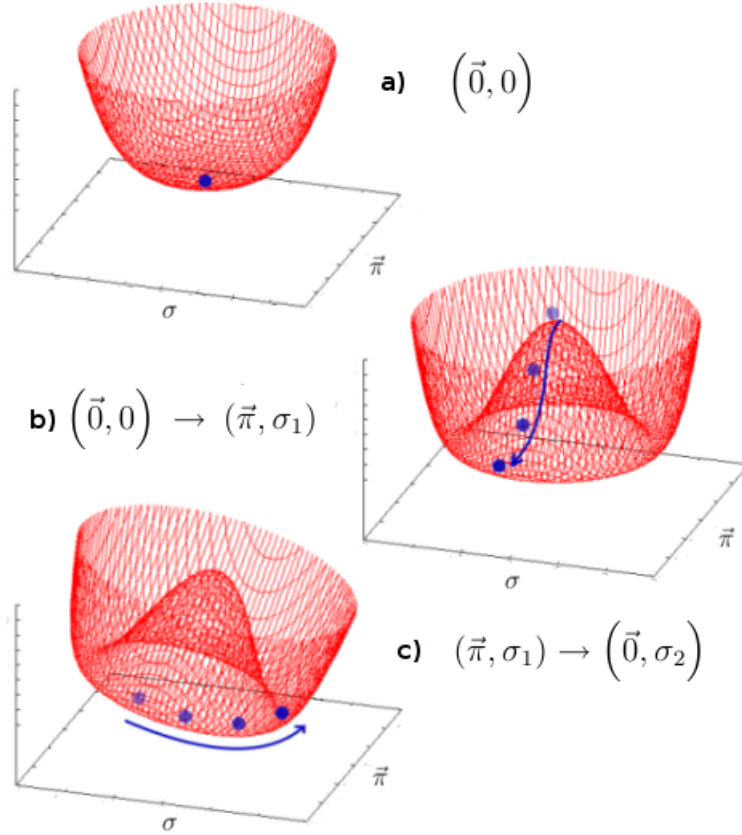


Figure 1.4: DCC evolution phases: a) extremely high temperatures \rightarrow chiral symmetry restoration; b) spontaneous breaking, explicit breaking suppressed; c) contact with ordinary vacuum \rightarrow explicit breaking;

Described scenario is illustrated on [Figure 1.4](#).

Quench Scenario

The hot debris located on the surface of the fireball might be represented as a source of the long-wavelength pionic excitation associated with the disoriented interior. Rajagopal and Wilczek [11] have realised that a strong long-wavelength pion field configuration could

be formed during the out-of-equilibrium chiral phase transition in the context of heavy-ion collisions. The rapid expansion of the system results in a rapid suppression of initial fluctuations (quenching) which results in a significant amplification of soft pion modes.

One can assume that a large amount of energy has been deposited in the collision zone, corresponding to a very high temperature (above the chiral transition temperature, $T_{ct} \approx 200$ MeV [12]). Due to the rapid expansion, this hot system is being rapidly cooled down, which results in a strong suppression of the initial thermal fluctuations. Rajagopal and Wilczek in their work assume an instantaneous quench from above to below the critical temperature at the initial time. The initial field configurations are sampled from a chirally symmetric probability distribution with the fluctuations frozen by hand.

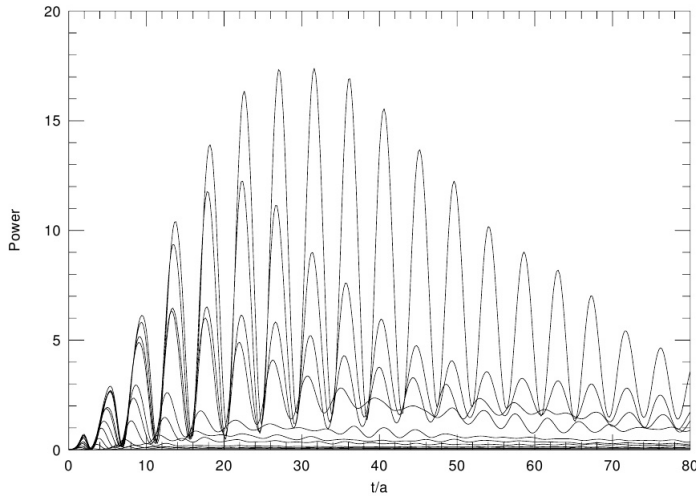


Figure 1.5: Power spectrum of the pion field as a function of time (in lattice units) for a given initial field configuration in the quench scenario. Low-momentum modes are dramatically amplified. Picture adopted from [11].

What they found is shown on Figure 1.5 - the pion field power spectra is due to the far-from-equilibrium initial condition dramatically amplified in low momentum modes.

Due to the very unstable initial state, which was assumed to be formed as a consequence of the rapid expansion, typical pion field configurations exhibit a significant amplification and strong long-wavelength pion field develops rapidly. Expansion causes an energy density drop-off and the dynamics might eventually linearise as the modes stop interacting. If such a freeze-out happens short enough after the collision, the system may be left in this strong field configuration and subsequently decay through coherent pion emission. This provides a microscopic scenario for the DCC formation in heavy-ion collisions.

1.2.3 DCC Signatures

Probably the most important signature for experimental physics is a different isospin distribution, e.g. the neutral pion fraction $f = \frac{\pi^0}{\pi^0 + \pi^+ + \pi^-}$. Under the normal conditions, pions are produced in 1:1:1 ratio, thus the neutral pion fraction is Gaussian, strongly peaked at 1/3. In the limit of large N it can be expressed as

$$p(f) = \delta(f - 1/3) \quad (1.39)$$

Not so in the DCC case.

We will start with an assumption that the state of the system is an isospin singlet and that all of the pions have same spatial wave functions. At first we will introduce creation and annihilation operators a_i^\dagger, a_i (where i is an isospin index: 1,2,3) which create or annihilate relevant pions. Let's add the condition of normalisation

$$[a_i, a_j^\dagger] = \delta_{ij} \quad (1.40)$$

The isospin operators can be then defined as

$$I_i = -i\varepsilon_{ijk} a_j^\dagger a_k \quad (1.41)$$

It is convenient to work in a basis where I_3 is diagonal. Therefore we will go over to the raising and lowering operators $a_\pm = \frac{1}{\sqrt{2}}(a_1 \pm ia_2)$ and $a_\pm^\dagger = \frac{1}{\sqrt{2}}(a_1^\dagger \pm ia_2^\dagger)$. Consequently

$$I_3 = a_+^\dagger a_+ - a_-^\dagger a_- \quad (1.42)$$

We will also introduce isospin raising/lowering operators

$$I_\pm = \pm\sqrt{2}(a_\pm^\dagger a_3 + a_3^\dagger a_\mp) \quad (1.43)$$

Now we will construct a iso-singlet multi-pion state $|\psi\rangle$ which is an eigenstate of the total pion number operator. Requirement of $I_3|\psi\rangle = 0$ results in condition $n_+ = n_-$. Therefore the total number of pions is an even integer. Thus we can expand

$$|\psi\rangle = \sum_{n=0}^N C_n^{(N)} (a_3^\dagger)^{2n} (a_+^\dagger a_-^\dagger)^{N-n} |0\rangle \quad (1.44)$$

where $2N$ is the total number of pions, $2n$ the number of neutral pions, $|0\rangle$ is annihilated by the operators a_i , $C_n^{(N)}$ are coefficients determined from the requirement of $I_\pm|\psi\rangle = 0$. From the relation $I_+|\psi\rangle = 0$ one gets N linear equations for $N + 1$ unknown coefficients. Thus all the coefficients can be rewritten in the terms of one unknown coefficient, e.g. $C_n^{(0)}$ (The equation $I_-|\psi\rangle = 0$ brings no additional conditions).

Since the operator $S^\dagger = 2a_+^\dagger a_-^\dagger - (a_3^\dagger)^2$ commutes with the isospin operators I_i , the state

$$|\psi\rangle = C_n^{(0)}(S^\dagger)^N |0\rangle \quad (1.45)$$

is a $2N$ pion iso-singlet and must be the most general such state in which all of the pions have the same spatial wave function. Hence it is obvious that the possibility of seeing $2n$ neutral pions out of $2N$ total pions in such a state is

$$P(n, N) = \frac{(N!)^2 2^{2N} (2n)!}{(2N+1)! (n! 2^n)^2} \quad (1.46)$$

For $N, n \gg 1$ one can use the Stirling's formula and get the following approximate result

$$P(n, N) \sim \sqrt{\frac{N}{n}} \quad (1.47)$$

This means the probability distribution of the neutral pion fraction f is approximately $p \sim \frac{1}{\sqrt{f}}$. More accurate approach [9] would yield the following distribution

$$p(f) = \frac{1}{2\sqrt{f}} \quad (1.48)$$

The above-mentioned distribution is strongly non Gaussian. For example, probability that maximally 10% of produced pions will be neutral is more than 30%. This causes anomalously large event-by-event fluctuations of the π_0 fraction.

What other DCC signals can we anticipate? It's a not-so-easy-to-answer question. Bjorken mentions in his "DCC Trouble List" [10] the following ones (many of them with a question mark):

- Excess at low p_T
- Clusters with low relative p_T
- "Core-less jets"
- Pion clusters of the same charge (Centauro events) ?
- Anomalies in correlation functions
- Anomalous bremsstrahlung ?
- Soft baryon/antibaryon production, via topological obstructions
- Amplification of isospin violation

But as we have said earlier, the most important signal/evidence is the inverse square-root distribution of the π_0 fraction and resulting event-by-event fluctuations.

1.2.4 Experimental Methods

We know yet what to search, but where and how? Many special methods have been developed during past years in order to reveal any possible traces of the DCC in high-energy collisions. These are the most promising ones:

Multi-Resolution Analysis (MRA)

This technique takes an advantage of discrete wavelet transformation (DWT) ⁶. It let us to scan the particle distribution at different length scales and subsequently to choose the one which indicates any eventual domain structures.

Much more place will be dedicated to the MRA in the next chapter, therefore I will advance to another procedures.

Event-shape Analysis

Event-shape analysis is based on the fact that the DCC presence should lead to an event-shape anisotropy. If we have two detectors (one for charged pions, the other one for photons from $\pi_0 \rightarrow \gamma\gamma$ decay) covering the same space area, a large number of charged particles detected by the first detector should be followed by low photon counts on the second detector in case of presence of a DCC domain.

In terms of the terminology used in flow analysis, a simple distribution of particles would result in the same flow direction in both detectors, with the flow angle difference peaking at zero. However, in the events where the neutral pion fraction has been modified according to the DCC probability distribution, the flow angles will be almost perpendicular to each other.

When applying on generated/experimental data, one starts with constructing two sums running over all particles in a given event

$$X = \sum_i \cos(2\phi_i) \quad (1.49)$$

$$Y = \sum_i \sin(2\phi_i) \quad (1.50)$$

where ϕ_i is the azimuthal position of the i^{th} particle. Then the flow angle Ξ is defined as

$$\Xi = \arctan\left(\frac{Y}{X}\right) \quad (1.51)$$

In an ideal case, the distribution of Ξ is (if the number of events is large enough) uniform from 0 to π , since the flow direction points randomly in each event. Nevertheless, when the events are realigned with respect to flow angle, two peaks at 0 and π appear in the distribution.

⁶Also other transformations can be used. Good example is the *Lorentz multi-resolution analysis* described in the next chapter.

Two detectors (charged particles vs. photons) with the same phase-space coverage will exhibit the same flow angles in the non-DCC case. Hence the distribution of $\Psi = \Xi_{ch} - \Xi_{\gamma}$ will be peaked at 0. On the other hand, if there are some DCC events, in a concrete area more charged particles will be detected than photons and the flow angles will differ from each other. Their difference Ψ will not display a peak at 0 anymore. Most probably it will be peaked at $\frac{\pi}{2}$. It can be shown [14] that this method is sensitive in cases when more than 10% of the events are of DCC-type. Unfortunately, it hasn't been used on experimental data yet.

Robust Observables

This method introduces a set of specific observables which are rather insensitive to the fluctuations of the total multiplicity, thus they are a good probe for the charged-to-neutral ratio fluctuations. They are also quite insensitive to detector efficiencies. The i^{th} robust observable is defined as ratio of so-called reduced bivariate factorial moments, however, it can be shown it is equal to

$$r_{i,1} = 2 \frac{\langle f(1-f)^i \rangle}{\langle (1-f)^{i+1} \rangle} \quad (1.52)$$

In case of a generic pion production (with neutral pion fraction distribution $p(f) = \delta(f - 1/3)$) it reads

$$r_{i,1} = 1 \quad (1.53)$$

for all i 's, because $\langle f^i \rangle = \langle f \rangle^i = (1/3)^i$. However, in case of an ideal DCC production, one gets

$$\langle f^i (1-f)^j \rangle = \frac{\Gamma(i+1/2)\Gamma(j+1)}{2\Gamma(i+j+3/2)} \quad (1.54)$$

and therefore

$$r_{i,1} = \frac{1}{1+i} \quad (1.55)$$

In other words, with the growing i the difference between $r_{i,1}(DCC)$ and $r_{i,1}(generic)$ is also growing.

This procedure has been developed and used for the DCC search by the MiniMAX collaboration at the Fermilab.

Φ -measure

Φ -measure of an observable is defined as

$$\Phi = \sqrt{\frac{\langle \left(\sum_{i=1}^N (x_i - \bar{x}) \right)^2 \rangle}{\langle N \rangle}} - \sqrt{(x - \bar{x})^2} \quad (1.56)$$

where the sum is running over all particles in one event, x is the value of the given observable in a given event, \bar{x} is averaged over all particles and events.

It can be shown [9] that for non-DCC events (with uncorrelated $N_{charged}$ and $N_{neutral}$) the Φ -measure is zero. Nevertheless, events with the ideal DCC production distinguishes itself with

$$\Phi_{DCC} = \sqrt{\frac{4 \langle N_{\pi} \rangle}{45}} - \sqrt{\frac{2}{9}} \quad (1.57)$$

1.2.5 Present Status

Despite of the fact that the DCC has been searched for about 15 years, no clear evidence of its existence has been submitted. This bring us to the question, if the disoriented chiral condensate exists at all. Actually, no contemporary theory does necessary need the DCC for its validity. On the other hand, all the unsuccessful attempts are explained by the fact that any DCC domains would be probably extremely small. These facts imply another important question. Is the DCC worth of looking for? I hope it is. It could provide us useful information about the structure of the QCD vacuum and about the chiral phase transition.

Chapter 2

Multi-Resolution Analysis

2.1 Multi-Resolution Wavelet Analysis

2.1.1 Description

Wavelet analysis (WA) applies discrete wavelet transformation, known from many other physical and mathematical disciplines (e.g. image processing), on experimental (or simulated) data in order to gain the ability to scan the particle distribution at different length scales and then to choose the one which indicates any interesting structures - eventual DCC domains. Such a procedure is called multi-resolution analysis.

The idea of using the discrete wavelet transformation (DWT) for the DCC search comes from Huang, Sarcevic, Thews and Wang [15]. They realised that there is a serious problem with the detection of the DCC. We know yet that the DCC pion probability distribution is $p(f) = \frac{1}{2\sqrt{f}}$, but if there is a large number of uncorrelated domains - which is actually quite plausible - the total distribution would become Gaussian, no matter what the original distribution looked like. This arises from the Central Limit Theorem. Therefore, the phase space has to be scanned locally. And the DWT is the tool which has such an ability.

DCC domains should be localised in coordinate space. If they develop collective motion in the course of their time evolution, they should also become localised in momentum space. Therefore it is convenient to divide the phase-space into small bins $\Delta\eta \Delta\phi$ (where *eta* stands for pseudorapidity and *phi* for azimuthal angle) and to define π_0 fraction f locally. Since position of a DCC domain is not fixed event-by-event, it is quite useful not to study the probability distribution $p(f)$ in each bin, but instead to study the probability of finding f in some particular interval $[f_1, f_2]$ in *all* bins of the same size in one event and to average over all events. Such a probability distribution will of course depend on the size of the bin.

The fraction f can be studied as a function of η or ϕ . In the following text I will denote it only $f(x)$, where x is a dimensionless variable defined on interval $[0, 1]$, namely $\phi/2\pi$ or $\eta/(\eta_{max} - \eta_{min})$. And the resolution is Δx . We will divide the space into 2^j bins

by assuming $\Delta x = 1/2^j$, where positive integer j satisfies $j < j_{max}$ for some j_{max} (most often $j_{max} = 4$). Let's denote value of f in the k^{th} bin

$$f_k^j = f(x = k\Delta x) \quad (2.1)$$

Consider a set of the following functions

$$\varphi_k^j = \begin{cases} 1 & \text{if } k/2^j \leq x < (k+1)/2^j \\ 0 & \text{otherwise} \end{cases} \quad (2.2)$$

One can sample the function f like

$$f^{(j)}(x) = \sum_{k=0}^{2^j-1} f_k^j \varphi_k^j(x) \quad (2.3)$$

where the coefficients f_k^j can be identified with the ones from (2.1). Notice that the functions $\varphi_k^j(x)$ can be derived from a single function $\varphi(x)$ - so-called *mother* (or also *scaling*) function

$$\varphi_k^j(x) = \varphi(2^j x - k) \quad (2.4)$$

In our case $\varphi(x) = \theta(x)\theta(1-x)$. Hence (2.3) is called mother function representation of the function f at scale j , the functions f_k^j are then called mother function coefficients (MFC's).

We can go to lower resolution by joining two neighbouring bins $2k$ and $2k+1$ into one of size $2\Delta x = 1/2^{j-1}$. Thus

$$\varphi_k^{j-1} = \varphi_{2k}^j + \varphi_{2k+1}^j \quad (2.5)$$

and f_k^{j-1} can be defined as

$$f_k^{j-1} = 1/2 (f_{2k}^j + f_{2k+1}^j) \quad (2.6)$$

The function $f(x)$ can be again resampled

$$f^{(j-1)}(x) = \sum_{k=0}^{2^{j-1}-1} f_k^{j-1} \varphi_k^{j-1}(x) \quad (2.7)$$

The information loss between two scales is encoded in the difference $\tilde{f}^{(j-1)}(x) = f^{(j)}(x) - f^{(j-1)}(x)$. The latter can be written as

$$\tilde{f}^{(j)}(x) = \sum_{k=0}^{2^j-1} \tilde{f}_k^j \psi_k^j(x) \quad (2.8)$$

where the functions $\psi_k^j(x)$ can be expressed in terms of the functions $\varphi_k^j(x)$.

$$\psi_k^j(x) = \varphi_{2k}^{j+1}(x) - \varphi_{2k+1}^{j+1}(x) \quad (2.9)$$

The equation (2.8) is now called father function representation with father function coefficients \tilde{f}_k^j (FFC's), since the functions $\psi_k^j(x)$ can be obtained from a single function $\psi(x)$ (called *father*, or sometimes *wavelet* function). In our case $\psi(x)$ would be equal to $\varphi(2x) - \varphi(2x - 1)$. For the FFC's the following relation reads

$$\tilde{f}_k^{j-1} = 1/2 (f_{2k}^j - f_{2k+1}^j) \quad (2.10)$$

The basis (2.2) is called Haar basis, since it is derived from the Haar function (Haar wavelet). This basis is very intuitive, but it has a serious disadvantage. Its mother function is discontinuous and therefore it cannot be localised in the scale space. Fortunately, modern mathematics is able to give us the wavelet bases which are well localised in the scale space. A large group of such wavelets was discovered by Ingrid Daubechies. Widely used is e.g. the D-4 wavelet [17]. Daubechies mother and father functions are defined as

$$\varphi(x) = \sum_m c_m \varphi(2x - m) \quad (2.11)$$

$$\psi(x) = \sum_m (-1)^m c_{1-m} \varphi(2x - m) \quad (2.12)$$

respectively. The Haar wavelet is also a simple Daubechies wavelet, with coefficients $c_0 = c_1 = 1/2$ (other c_m 's are zero). Coefficients of the D-4 wavelet are

$$\begin{aligned} c_0 &= \frac{1 + \sqrt{3}}{4} & c_1 &= \frac{3 + \sqrt{3}}{4} \\ c_2 &= \frac{3 - \sqrt{3}}{4} & c_3 &= \frac{1 - \sqrt{3}}{4} \end{aligned}$$

All other c_m 's are zero.

Application

The question is how to use the DWT in order to find DCC events. We know that the information about the original (input) function is partially saved in the MFC's, the rest of the information (the information loss between two scales) is saved in the FFC's. Hence it can be useful to study the MFC and (or) FFC distributions when one is looking for the DCC.

Authors of [15] made a simulation with 500 random events and 500 DCC-like events and plotted the distribution of the MFC's for scales $j = 0, 1, 2, \dots, 7$. In both cases the distribution was hyperbolic for the finest scale ($j = 7$) and overcame to the Gaussian for lower j 's (as one would expect from the central limit theorem). The Gaussian distribution was narrower and narrower for the lowest j 's. The difference between the random sample and the DCC sample was in the "speed" with which this change happened. In the DCC case there was a *delay*. E.g. the Gaussian distribution at scale $j = 0$ was in the DCC case as wide as the one at scale $j = 3$ of the random sample.

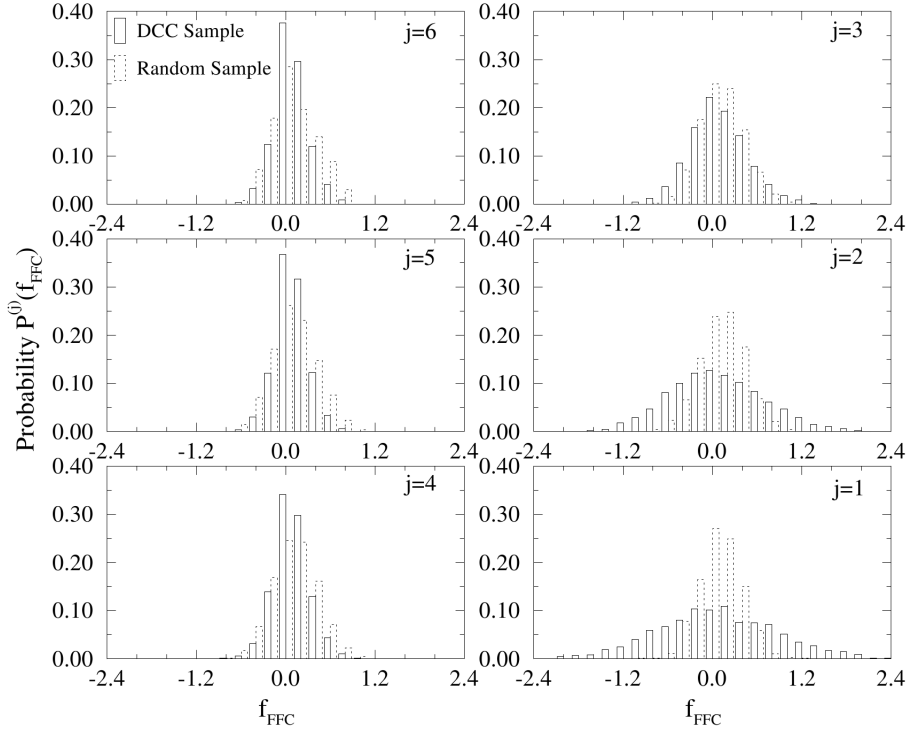


Figure 2.1: Distribution of the FFC's obtained from a sample of 500 random events (dashed line) and 500 DCC-like events (solid line) at various scales. Picture adopted from [15].

For the father function coefficients the situation becomes yet more interesting. The MFC's at scale j contain also information from all finer scales. Hence fluctuations at one scale can be suppressed by other fluctuations at a finer scale. FFC's include information only from one scale, since they are the difference of the MFC's at that scale and one finer scale. Distributions of the FFC's for the previously mentioned 500 random and 500 DCC-like events are plotted on Figure 2.1. Differences between the random events and the DCC events are clearly visible.

2.1.2 Wavelet Analysis in Particular Experiments

WA98

The WA98 was a general-purpose large-acceptance photon and hadron spectrometer at the CERN SPS with the ability to measure several global observables in Pb+Pb collisions event-by-event. The experimental setup is shown on Figure 2.2.

One of the tasks performed on the WA98 was searching for the DCC. During the experiment photon and charged multiplicities were measured by the Photon Multiplicity Detector (PMD) and Silicon Pad Multiplicity Detector (SPMD) in each event. Also

the centrality of the collision was determined from the transverse energy measurement in the Midrapidity Calorimeter (MIRAC). The PMD covered the pseudorapidity region $2.8 < \eta < 4.4$. The SPMD was detecting charged particles in the region $2.35 < \eta < 3.75$.

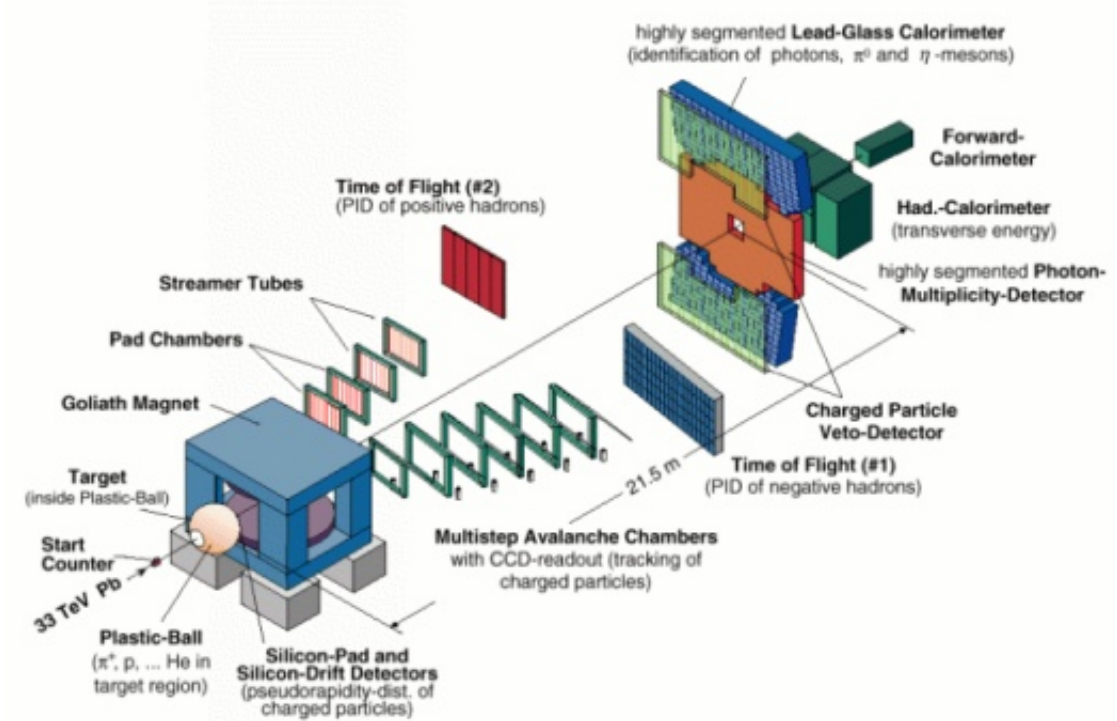


Figure 2.2: Setup of the WA98 experiment at the SPS. Picture adopted from the WA98 official web site [21].

During one particular analysis [18] the photon fraction

$$f(\phi) = \frac{N_{\gamma-like}(\phi)}{N_{\gamma-like}(\phi) + N_{ch}(\phi)} \quad (2.13)$$

(as a function of the azimuthal angle ϕ) was used as the input for the discrete wavelet transform with the D-4 wavelet bases. Maximal resolution was $j_{max} = 5$. The sample function (2.13) was analysed at different scales ($j = 5, 4, 3, 2, 1$) and the father function coefficients were obtained for each scale ($j = 4, 3, 2, 1$) from the distribution of the sample function at one higher scale (see equation (2.10)). Distribution of these FFC's was then compared with the FFC's of mixed events and events generated with the VENUS and GEANT event generators.

Any significant presence of non-statistical localised fluctuations in the data should increase the rms deviation of the distribution of the FFC's and could consequently result in non-Gaussian tails.

There were three types of mixed events made: minimally, partially and maximally mixed events.

Maximally mixed events (M1) were constructed by mixing hits in PMD and SPMD separately, but still satisfying the real event global $N_{\gamma\text{-like}} - N_{ch}$ correlation. For each mixed event $N_{\gamma\text{-like}}$ hits were randomly selected from all γ -like hits from all events and N_{ch} hits were randomly selected from all charged hits from all events. Such mixed events should have been most sensitive to the presence of localised fluctuations.

Minimally mixed events (M2) contained hits of the charged particles from one event and photon hits from another event. These mixed events kept the individual localised fluctuations in $N_{\gamma\text{-like}}$ or N_{ch} , but removed event-by-event localised correlated fluctuations between them. Comparison of these mixed events to real ones could have revealed correlated localised fluctuations between $N_{\gamma\text{-like}}$ and N_{ch} .

Partially mixed events (M3- γ , M3- ch) were the intermediates between the maximally and minimally mixed events. They mixed hits from one detector, but contained the structure of hits in the second detector. By comparison of these events to the real events one could have seen the localised fluctuations in N_{ch} or $N_{\gamma\text{-like}}$ separately.

Obtained FFC distributions are shown in [Figure 2.3](#). On the next figure also the rms deviations of the FFC's are reprinted.

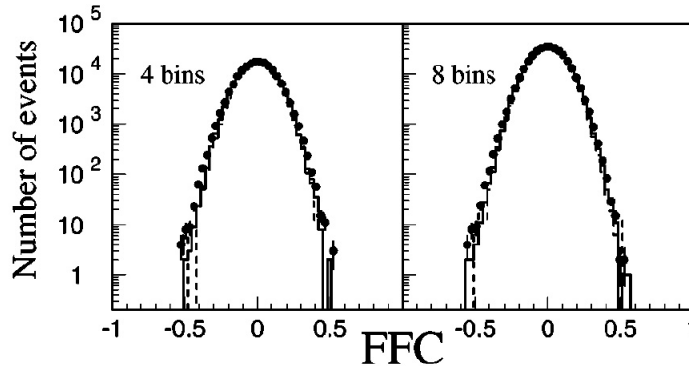


Figure 2.3: Distribution of the FFC's for ϕ divided into 4 and 8 bins. Solid circles represent experimental data, solid and dashed histograms represent M1 and V+G events respectively. Picture adopted from [\[18\]](#).

How can be these results interpreted? On [Figure 2.3](#) one can see that the experimental data make up a FFC distribution with broader tails than the distribution obtained from generated and M1-mixed events. This can be a signature of some non-statistical fluctuations. However, its shape doesn't correspond to the one anticipated for DCC-like events. Also the rms deviations of the experimental data don't differ too much from those for M1 events. There should be much more significant difference for the DCC-like events. Thus it is difficult to identify the source of these fluctuations. In this light it comes as no surprise that the authors of [\[18\]](#) end up their report with the following words: "The interpretation of the result remains an open question."

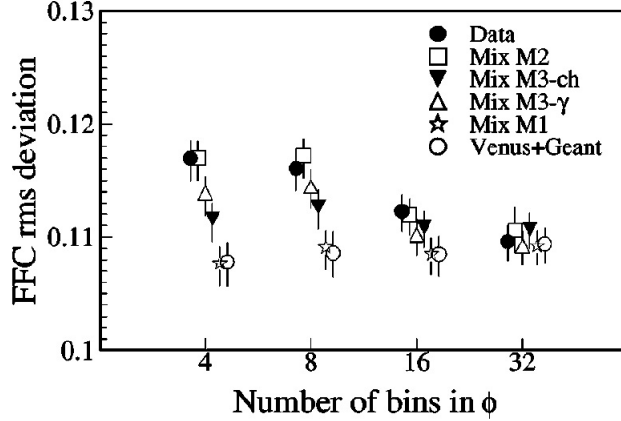


Figure 2.4: FFC rms deviations for ϕ divided into 4, 8, 16 and 32 bins.

2.2 Multi-Resolution Lorentz Analysis

2.2.1 Description

Motivation

The wavelet analysis could be a useful method which can help us in searching for the DCC. However it suffers from a difficulty. When applying the DWT, one has to divide the phase-space into bins by setting borders between the bins. If a potential DCC domain would be splitted by these borders, there is a real threat that one won't be able to reconstruct and recognise such a domain. Thus the discrete wavelet transform has to be made repeatedly, each time with various binning, in order to avoid this problem.

The aforementioned inconvenience led V. Petráček [16] to develop another type of the multi-resolution analysis which would overcome the problem with the binning.

Cauchy-Lorentz Distribution

The method uses of the **Cauchy-Lorentz** distribution function - therefore I call this method the multi-resolution Lorentz analysis (MRLA). The basic idea is following: Each particle hit (position) can be represented as a 2D delta function over the phase-space. But what if we replace the delta function by a Cauchy-Lorentz function that is only approaching the delta function? Then we could make operations that are *forbidden* for delta functions, like summing up the functions. Such a sum would be greatest for areas where the particles are close together and their Lorentz functions overlap. Hence size of this sum could point to a DCC domain presence.

For our purposes we will use the Cauchy-Lorentz function of the form

$$\mathcal{L}_k^{(j)}(\phi, \eta) = c \cdot \frac{\varepsilon_j |Q_k|}{\varepsilon_j^2 + (\phi - \phi_k)^2 + (\eta - \eta_k)^2} \quad (2.14)$$

where c is a scaling constant, ϕ_k and η_k specify position of the k^{th} particle in the detector, $|Q_k|$ is absolute value of charge of the k^{th} particle (in units of the elementary charge), ε_j is the resolution at current scale j ($j = 0, 1, 2, \dots, j_{max}$)

$$\varepsilon_j = \frac{k_1}{k_2^j} \quad (2.15)$$

where k_1, k_2 are some constants. It is obvious that the constant c determines only height of the Lorentz function whereas ε_j determines both the height and width.

Finally, we can sum over all particles and get the result

$$L^{(j)}(\phi, \eta) = \sum_{k=1}^{N_{hits}} \mathcal{L}_k^{(j)}(\phi, \eta) \quad (2.16)$$

If we set a reasonable threshold, all ϕ - η areas where $L(\phi, \eta)$ overruns this threshold will become interesting for us since they can contain possible particle domains.

Like in the [section 2.1](#), one can define a new function $F^{(j)}$ as the difference of functions L at two adjacent scales.

$$F^{(j)} = L^{(j+1)} - L^{(j)} \quad (2.17)$$

Using the terminology of the [section 2.1](#), one can call the function L the **mother function** whereas the function F can be called the **father function**. Once again, the father function give us the information only about the fluctuations at one scale which makes it more useful.

Let's return to [Equation 2.14](#) once more. The expression $|Q|$ in the numerator ensures we encounter only the charged hits whereas the neutral hits are neglected. This is extremely convenient since the reconstruction of the neutral pions from their decay products (photons) is much less accurate than the detection of the charged pions. Unfortunately, one can proceed this way only if the (charged + neutral) hit density is approximately the same in the whole phase-space. Otherwise areas with the higher particle density would appear as if there was a larger fraction of charged particles and such an area could be incorrectly treated as a DCC domain. Therefore the amplitude of the mother function L has to be rescaled in accordance with the hit density $n(\phi, \eta)$

$$L^{(j)}(\phi, \eta) = \frac{1}{n(\phi, \eta)} \sum_{k=1}^{N_{hits}} \mathcal{L}_k^{(j)}(\phi, \eta) \quad (2.18)$$

2.2.2 Application of MRLA on Simulated Events

I have tested MRLA method on simulated DCC events with various proprieties. Events (background) have been generated with the PYTHIA 8.1 event generator. DCC domains were added manually, satisfying the condition [\(1.48\)](#). Obtained data were analysed with ROOT 5.

As an input for the analysis the ϕ and η coordinates of π^+ , π^- and π^0 ¹⁾ hits have been used. On the output I have obtained 3D histograms of the functions (2.16) and (2.17). Actually, function (2.16) had to be changed slightly in order to take different hit densities into account (remember equation (2.18)).

$$L^{(j)}(\phi, \eta) = \sum_{k=1}^{N_{hits}} c \cdot \frac{\varepsilon_j \Delta_k}{\varepsilon_j^2 + (\phi - \phi_k)^2 + (\eta - \eta_k)^2} \quad (2.19)$$

where

$$\Delta_k = \begin{cases} +1 & \text{for } \pi^\pm \\ -2 & \text{for } \pi^0 \end{cases} \quad (2.20)$$

This ensures that the main value of the mother function (2.19) will be approximately zero for events with the pions produced in the 1:1:1 ratio. The father function is still obtained as a difference of two mother functions (2.19) at two adjacent scales.

Non-DCC Case

On Figure 2.5 you can see, how such a histogram looks for a non-DCC event. It is quite

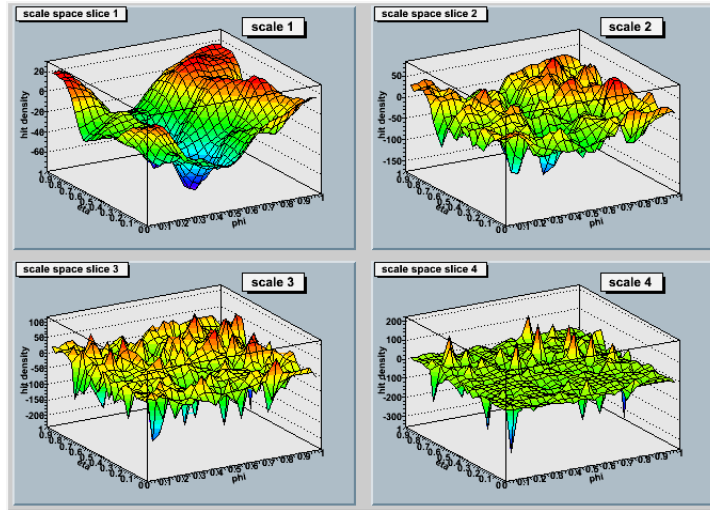


Figure 2.5: Mother function of a non-DCC event at 4 various scales. Coordinates ϕ and η are displayed in relative units (for ϕ $0 = -\pi$ rad and $1 = \pi$ rad, for η $0 = -6$ and $1 = 6$).

evident that there are no significant peaks which would imply the presence of a charged pion domain.

¹⁾PYTHIA has been run with “no π^0 decay” option turned on. Otherwise π^0 hits would have to be reconstructed from photon hits.

1 DCC Domain

I have generated the DCC domains in two ways. One way was to only replace the original (PYTHIA) pions for pions satisfying the condition (1.48) in some small region. Such a domain has to be large enough in order to ensure that it contains a large number of pions which exhibit non statistical fluctuations of the neutral fraction. For events with ~ 400 particles the domain had to cover at least an area of 0.2×0.1 in relative units²⁾ (other words, the domain had to contain ~ 10 particles). This is shown on Figure 2.6. “Detected domains”

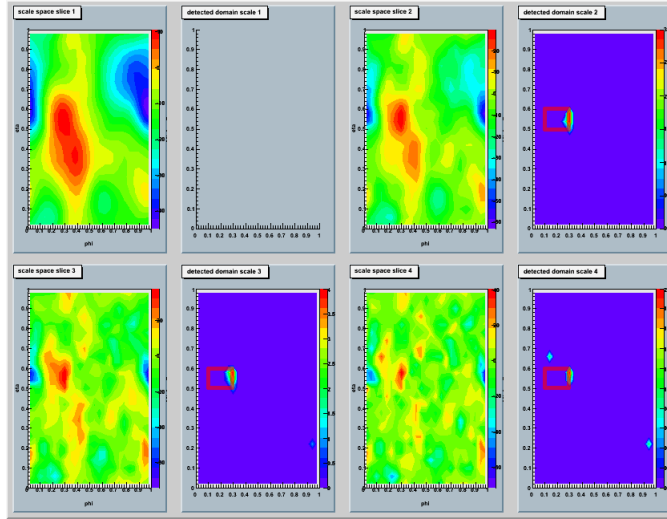


Figure 2.6: Mother function (slice in the ϕ and η plane) of a DCC event and detected domains at 4 various scales. Red rectangular denotes the real position of the domain.

are areas where the value of $L^{(j)}$ overruns a threshold value ($threshold = mean + k \cdot \sigma$; in our case $k = 2.2$). The domain was detected only for higher scales. This means it is not very significant. The same can be done for the father function (Figure 2.7).

Another way of creating a DCC domain was to add additional pions satisfying the condition (1.48). For events with ~ 400 pions the minimal number of added pions was approx. 60, otherwise the domain was not detected. See Figure 2.8. Unfortunately, the results are not very convincing.

Much better results have been achieved for 80 additional pions (Figure 2.9, Figure 2.10, Figure 2.11, Figure 2.12).

2 DCC Domains

Probably the biggest potential of this method is the ability to detect more than 1 domain in one event. An example is shown on Figure 2.13 and Figure 2.14. Each domain contains 80 pions, the background is made of ~ 400 pions. The pictures don't need any further

²⁾relative units: for ϕ : $0 = -\pi$ rad and $1 = \pi$ rad, for η : $0 = -6$ and $1 = 6$

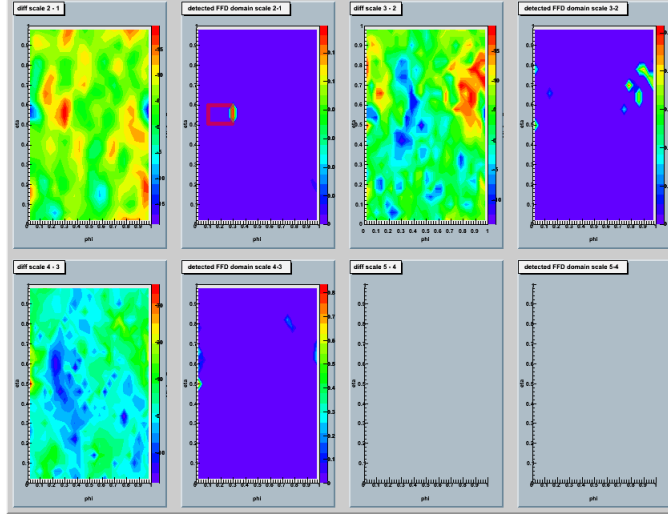


Figure 2.7: Father function (slice in the ϕ and η plane) of a DCC event and detected domains at 3 various scales. Red rectangular denotes the real position of the domain.

comments

Just for the completeness, there are some values that have been used for the calculations: $\varepsilon_j = 3/2^j$, the phase space has been divided into a net of 25×25 points, $L^{(j)}(\phi, \eta)$ has been calculated for each node of this net. This means in each node contributions to $L^{(j)}$ have been summed up. However, for faster algorithmus and more significant results not all contributions, but only ones from hits up to the distance $d = x \cdot 15 \cdot \frac{1}{2^j}$ (where x is the distance between two nodes, $x = 1/25$) have been summed up.

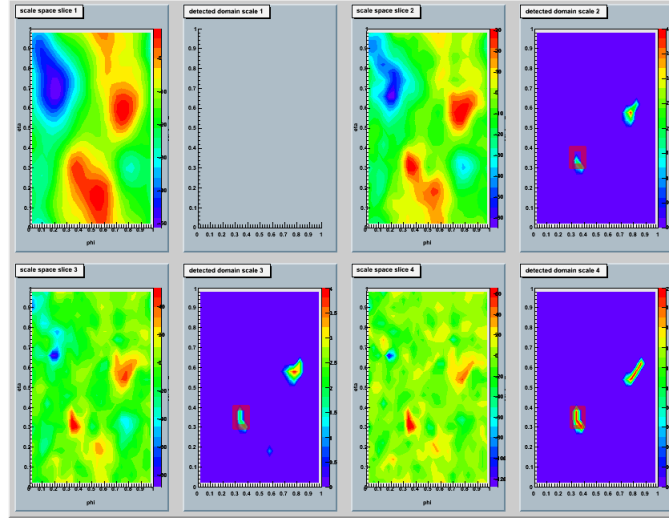


Figure 2.8: Mother function (slice in the ϕ and η plane) of a DCC event and detected domains at 4 various scales. Red rectangular denotes the real position of the domain.

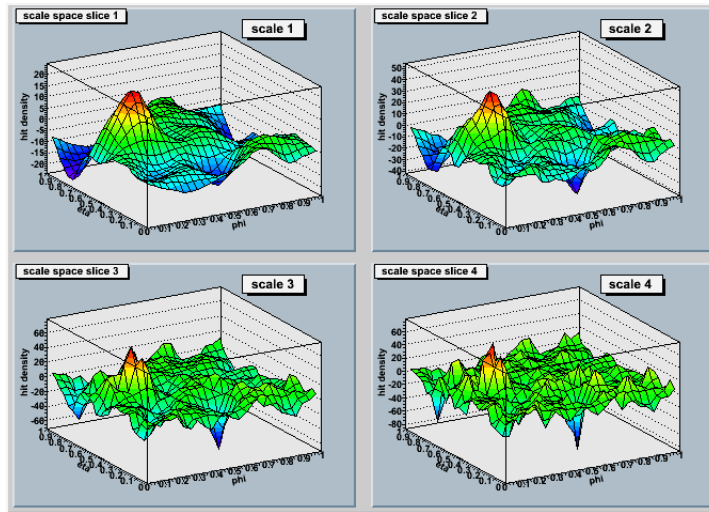


Figure 2.9: Mother function of a DCC event at 4 various scales (domain:80 pions, background: 400).

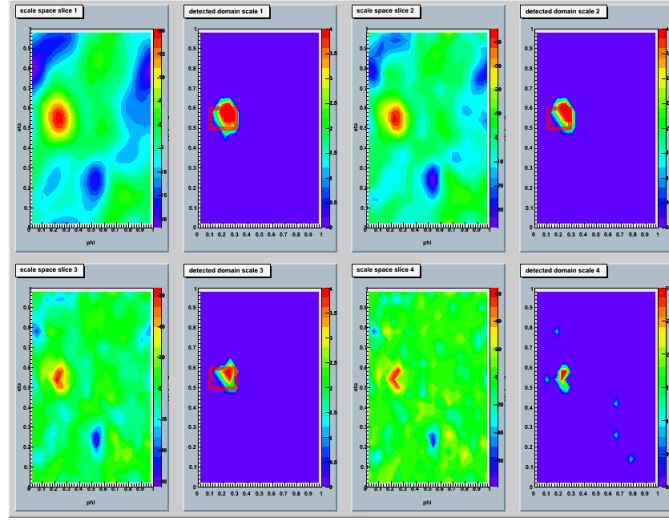


Figure 2.10: Mother function (slice in the ϕ and η plane) of a DCC event and detected domains at 4 various scales. Red rectangular denotes the real position of the domain.

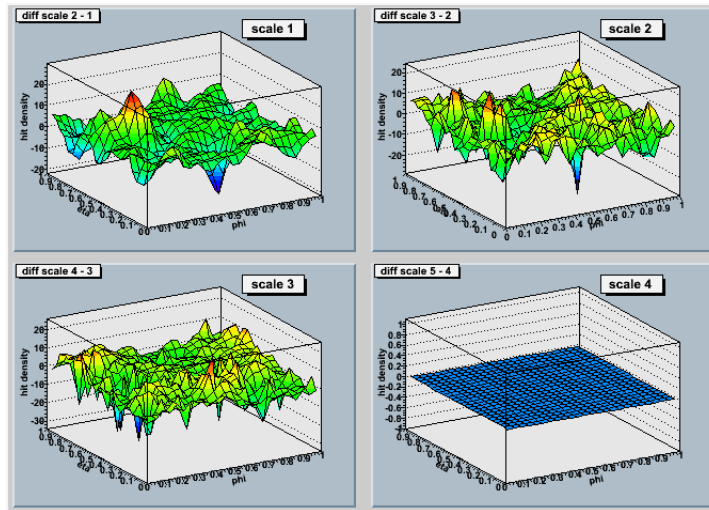


Figure 2.11: Father function of a DCC event at 3 various scales (domain:80 pions, background: 400).

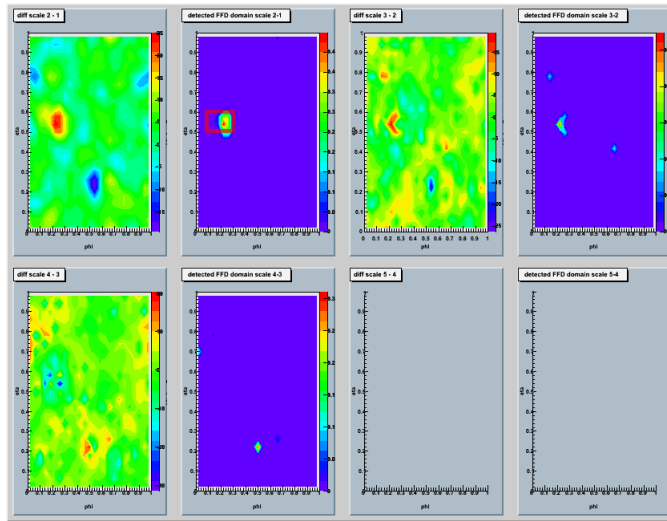


Figure 2.12: Father function (slice in the ϕ and η plane) of a DCC event and detected domains at 3 various scales. Red rectangular denotes the real position of the domain.

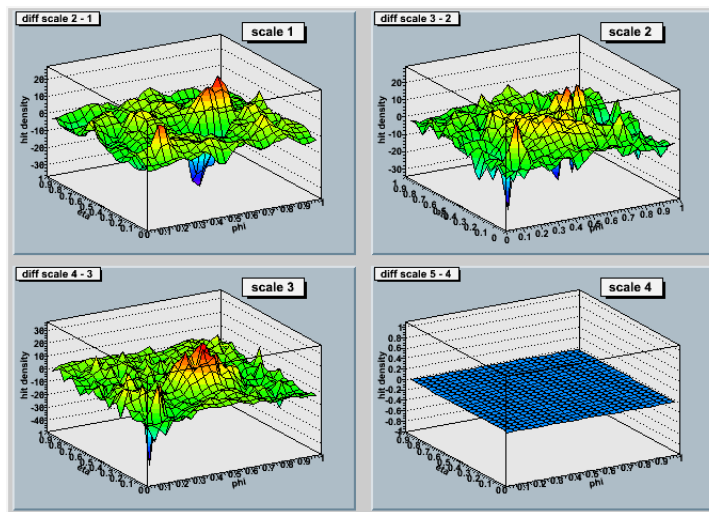


Figure 2.13: Father function of a DCC event with 2 DCC domains at 3 various scales.

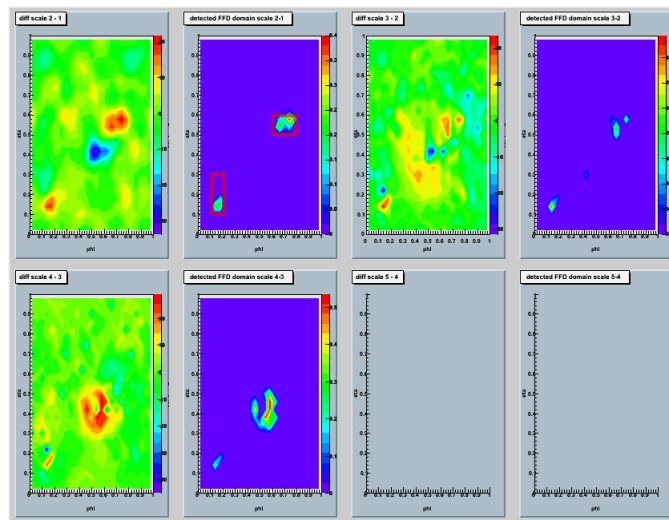


Figure 2.14: Father function (slice in the ϕ and η plane) of an event with 2 DCC domains at 3 various scales.

Chapter 3

ALICE Experiment

3.1 Introduction

A Large Ion Collider Experiment, or just **ALICE**, is a heavy-ion general-purpose detector operating at the Large Hadron Collider (LHC) at CERN. The ALICE Collaboration involves more than 1000 members from 109 institutes in 31 countries. Their aim is exploit the unique physics potential of nucleus-nucleus interactions at LHC energies and to study the physics of strongly interacting matter at extreme energy densities, where the formation of a new phase of matter, namely the quark-gluon plasma, is expected. Nuclear collisions at ultra-relativistic energies will be studied with sensitivity to the most of known observables in this experiment.

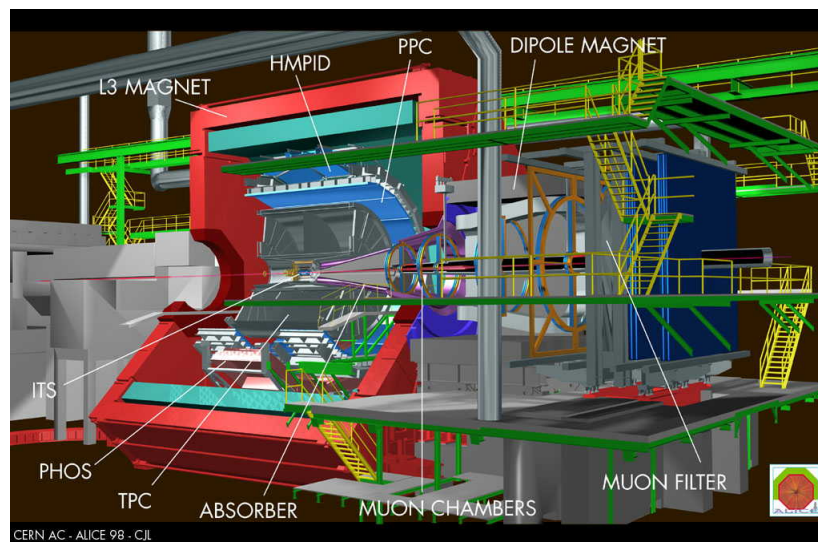


Figure 3.1: The ALICE detector scheme. ITS - Inner Tracking System, TPC - Time Projection Chamber, PPC - Parallel Plate Chambers (a time-of-flight detector), HMPID - High Momentum Particle Identification detector, PHOS - Photon Spectrometer. Picture adopted from [22].

3.2 Detector Overview

ALICE is a very complicated installation. The main sub-detectors are shown on [Figure 3.1](#). I will present here only their simple description. More detailed information can be found e.g. in [\[24\]](#).

3.2.1 ITS

Inner Tracking System (ITS) is the ALICE's innermost sub-detector system. It contains 2+2+2 layers of silicon pixel detectors (at radii $r = 3.9\text{cm}$ and $r = 7.6\text{cm}$), silicon drift detectors ($r = 14, 24\text{cm}$) and double-sided silicon micro-strip detectors ($r = 40, 45\text{cm}$) with total area 6.6m^2 . It covers pseudo rapidity range $|\eta| < 0.9$ for all vertices in the interaction diamond. Main purposes of the ITS is secondary vertex reconstruction of charm and hyperon decays and stand-alone track finding of low- p_T particles (down to $20\text{ MeV}/c$ for electrons). More over it provides momentum reconstruction of the low-energy particles and their identification (via dE/dx) in the non-relativistic region, it also improves the momentum resolution at large momenta.

Pixel detectors are unique because of their high granularity and excellent two-track resolution. Therefore they were used as the innermost layers.

The silicon drift detectors (SDDs) exploit the measurement of the transport time of charge deposited by a traversing particle to localise the impact point in one dimension, hence they enhance resolution and multi-track capability at the expense of speed. Thus they are well prepared for low event rates coupled with high particle multiplicities. The SDDs will be mounted on linear structures called ladders, each holding 5 detectors for layer 3, and 8 detectors for layer 4. The layers will be composed of 14 and 22 ladders, respectively.

The silicon strip detectors (SSD) are necessary for connecting of tracks from the ITS to the TPC. The detectors can be produced in large quantities in industry which makes them sufficiently cheap.

3.2.2 TPC

The Time Projection Chamber (TPC) is the main tracking detector of ALICE. It features large acceptance, which will enable us to analyse individual events and perform charged particle identification and its momentum and track analysis in the area $|\eta| < 0.9$. The chamber is filled with 90% Ne and 10% CO_2 . Its tracking efficiency is more than 90%.

3.2.3 TRD

TRD stands for Transition-Radiation Detector. Its goal is the electron identification in the central barrel with momenta greater than $1\text{ GeV}/c$, where the pion rejection capability of the TPC is not sufficient. Information from the high- p_T electrons measurement can be useful in identification of open charm and open beauty production in the collision.

3.2.4 TOF

In ALICE, there are used two types of time of flight (TOF) systems: Pestov spark counters and parallel plate chambers. Their main purpose is particle identification in energy region $0.2 - 2.5 \text{ GeV}/c$.

3.2.5 HMPID

HMPID, High-Momentum Particle Identification Detector, is designed as a single-arm array with an acceptance of 5% of the central barrel phase-space. It provides an inclusive measurement of identified hadrons for energies $p_T > 1 \text{ GeV}/c$. It extends the useful range for π/K and K/p differentiation up to $3 \text{ GeV}/c$ and $5 \text{ GeV}/c$ respectively. The detector consists of seven modules of RICHs (Ring Imaging Cherenkov) counters. Low chromacity C_6F_{14} is used as the radiator.

3.2.6 PHOS

PHOS is an abbreviation of PHOton Spectrometer. It is an electromagnetic spectrometer with very high resolution. It covers pseudorapidity region $-2.4 < \eta < 2.4$ and 100° in the azimuthal angle. It consist of two parts: electromagnetic calorimeter (EMCA) and charged particle veto (CPV) which excludes charged particle from EMCA's data. PHOS is used for photon and neutral particle (via photon decay) detection.

3.2.7 FMS

Forward Muon Spectrometer consists of a passive absorber which's task is to absorb hadrons and photons, high granularity tracking system of 10 detection planes, large dipole magnet (with $B = 0.7 \text{ T}$) and passive muon filter wall and four planes of trigger chambers.

3.2.8 PMD

Photon Multiplicity Detector measures photon multiplicity and spatial distribution on event-by-event basis. It provides estimates of transverse electromagnetic energy. PMD is displaced in the forward region, 360 cm from the interaction point. It covers pseudorapidity region of $2.3 < \eta < 3.5$.

3.2.9 FMD

Similarly to PMD, Forward Multiplicity Detector (FMD) enable us to study charged particle multiplicity fluctuations event-by-event. The pseudorapidity regions $-3.4 < \eta < -1.7$ and $1.7 < \eta < 5.1$ are covered by the forward multiplicity detector.

3.2.10 ZDC

Zero-Degree Calorimeter (ZDC) measures the total energy carried out of the collision in the forward direction. This help us to determine the centrality of the collision, since central collisions are significant with a large transversal energy release, on the other hand, after a non-central collision most of the energy is carried away in the forward and backward direction.

3.2.11 T0 and V0

These two small detectors serve as triggers for the other detectors. Each of them has two parts working in a coincidence.

3.3 ALICE and DCC

Can the experiment ALICE bring a new light to the DCC scene? Definitely YES, I believe.

ALICE will be studying heavy ion collisions at extremely high (never before reached) energies per nucleon¹⁾. This could provide sufficient conditions for a DCC domain(s) to form. What more, precise tracking system (ITS+TPC) and particle identification combined with the FMD and PMD detectors enable to easily apply the sophisticated analytical methods described in the previous chapter on gathered data.

An optimist would probably predict that it is only a question of a few months²⁾ to discover the disoriented chiral condensate.

¹up to 2.76 TeV/nucleon for Pb-Pb collisions

²written in July 2008

Summary and Conclusion

I have outlined a basic concept of the chiral symmetry and consequential mechanisms of the disoriented chiral condensate (DCC) formation. Detection of DCC domains is not trivial. Therefore two interesting analytical methods (multi-resolution wavelet analysis (MRWA) and multi-resolution Lorentz analysis(MRLA)) have been introduced. At the end a basic description of the experiment ALICE has been provided, since it is a plausible candidate for the discovery of the DCC.

Performed simulations in [section 2.2](#) shows that the multi-resolution Lorentz analysis is a usable tool for the DCC domain detection. Its great advantage lies in its ability to detect multiple domains in one event. But like everything new, it has to be adjusted and tested for the real data. That will be the touchstone.

Bibliography

- [1] J. Kapusta, B. Muller, J. Rafaeelski: *Quark-Gluon Plasma*, Elsevier, 2003
- [2] J. Letessier, J. Rafaeelski: *Hadrons and Quark-Gluon Plasma*, Cambridge Univ. Press, 2002
- [3] C.-Y. Wong: *Introduction to High-Energy Heavy-Ion Collisions*, World Scientific, 1994
- [4] Particle Data Group: *Review of Particle Physics*, 2006
- [5] V. Koch, Int.J.Mod.Phys. **E6**, (1997) 203-250
[arXiv:nucl-th/9706075v2](https://arxiv.org/abs/nucl-th/9706075v2)
- [6] S. Scherer, M. R. Schindler: *A Chiral Perturbation Theory Primer*, Mainz, 2005
[arXiv:hep-ph/0505265v1](https://arxiv.org/abs/hep-ph/0505265v1)
- [7] G. Ecker: *Chiral Symmetry*, Wien, 1998
[arXiv:hep-ph/9805500v1](https://arxiv.org/abs/hep-ph/9805500v1)
- [8] H. Dass: *Three Lectures on Chiral Symmetry*, Chennai, 2005
[arXiv:hep-ph/0506169v1](https://arxiv.org/abs/hep-ph/0506169v1)
- [9] B. Mohanty, J. Serreau, Phys.Rept. **414**, (2005) 263-358
[arXiv:hep-ph/0504154v2](https://arxiv.org/abs/hep-ph/0504154v2)
- [10] J. D. Bjorken: *A DCC trouble list*, Workshop on Disoriented Chiral Condensates (1996), Trento, Italy
<http://www-minimax.fnal.gov/talks/trento.ps>
- [11] K. Rajagopal, F. Wilczek, Nucl.Phys. **B404** (1993) 577-589
[arXiv:hep-ph/9303281v1](https://arxiv.org/abs/hep-ph/9303281v1)
- [12] P. N. Meisinger, T. R. Miller, M. C. Ogilvie: *A Phenomenological Treatment of Chiral Symmetry Restoration and Deconfinement*, 2002
[arXiv:hep-lat/0208073v1](https://arxiv.org/abs/hep-lat/0208073v1)
- [13] K. L. Kowalski, C. C. Taylor: *Disoriented Chiral Condensates: A White Paper for the Full Acceptance Detector at the SSC*, Cleveland, 1992
[arXiv:hep-ph/9211282v1](https://arxiv.org/abs/hep-ph/9211282v1)

- [14] B. K. Nandi, G. C. Mishra, B. Mohanty, D. P. Mahapatra, T. K. Nayak, Phys.Lett. **B449**, (1999) 109-113
[arXiv:nuclex/9812004v1](https://arxiv.org/abs/nuclex/9812004v1)
- [15] Z. Huang , I. Sarcevic, R. Thews, X.-N. Wang, Phys.Rev. **D54**, (1996) 750-758
[arXiv:hep-ph/9511387v1](https://arxiv.org/abs/hep-ph/9511387v1)
- [16] V. Petráček: *Study of heavy ion collisions with ALICE experiment at LHC*, Prague, 2007
- [17] S. Mallat: *A Wavelet Tour of Signal Processing*, Elsevier, 1999
- [18] The WA98 Collaboration, Phys.Rev. **C64**, (2001) 011901 R
- [19] The WA98 Collaboration, Phys.Rev. **C67**, (2003) 044901
- [20] The WA98 Collaboration, Phys.Lett. **B420**, (1998) 169-179
[arXiv:hep-ex/9710015v1](https://arxiv.org/abs/hep-ex/9710015v1)
- [21] WA98 Home Page
<http://wa98.web.cern.ch/WA98/>
- [22] Experiment ALICE Home Page
<http://aliceinfo.cern.ch>
- [23] M. Petráň: *Quark-gluon plasma and study of its properties in ALICE experiment at LHC*, Prague, 2006
- [24] *Technical Proposal for A Large Hadron Collider Experiment at the CERN LHC*, CERN/LHCC/95-71, CERN Pres, 1995

Acknowledgements

I would like to thank to doc. Vojtěch Petráček for his guidance and help with this work. Also I would like to thank to Radek Šmákal for his advices and suggestions. Finally I want to thank to Václav Zycháček for his “Lion Theme” front page.